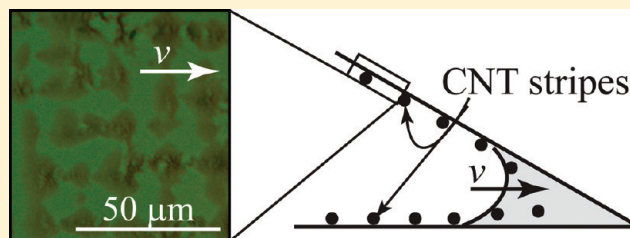


## Surface-Induced Patterns from Evaporating Droplets of Aqueous Carbon Nanotube Dispersions

Hongbo Zeng,<sup>\*,†,‡</sup> Kai Kristiansen,<sup>†,§</sup> Peng Wang,<sup>||,⊥</sup> Joakim Bergli,<sup>#</sup> and Jacob Israelachvili<sup>\*,§</sup><sup>†</sup>Department of Chemical and Materials Engineering, University of Alberta, Edmonton, Alberta T6G 2V4, Canada<sup>§</sup>Department of Chemical Engineering, Materials Research Laboratory, <sup>||</sup>Bren School of Environmental Science and Management, University of California, Santa Barbara, California 93106, United States<sup>#</sup>Department of Physics, University of Oslo, 0316 Oslo, Norway

**ABSTRACT:** Evaporation of aqueous droplets of carbon nanotubes (CNTs) coated with a physisorbed layer of humic acid (HA) on a partially hydrophilic substrate induces the formation of a film of CNTs. Here, we investigate the role that the global geometry of the substrate surfaces has on the structure of the CNT film. On a flat mica or silica surface, the evaporation of a convex droplet of the CNT dispersion induces the well-known “coffee ring”, while evaporation of a concave droplet (capillary meniscus) of the CNT dispersion in a wedge of two planar mica sheets or between two crossed-cylinder sheets induces a large area ( $>\text{mm}^2$ ) of textured or patterned films characterized by different short- and long-range orientational and positional ordering of the CNTs. The resulting patterns appear to be determined by two competing or cooperative sedimentation mechanisms: (1) capillary forces between CNTs giving micrometer-sized filaments *parallel* to the boundary line of the evaporating droplet and (2) fingering instability at the boundary line of the evaporating droplet and subsequent pinning of CNTs on the surface giving micrometer-sized filaments of CNTs *perpendicular* to this boundary line. The interplay between substrate surface geometry and sedimentation mechanisms gives an extra control parameter for manipulating patterns of self-assembling nanoparticles at substrate surfaces.



## ■ INTRODUCTION

Self-assembled patterns of polymers, carbon nanotubes (CNTs), and nano- and microparticles on surfaces have attracted great research interest recently in modern chemical synthesis, processing, and materials science,<sup>1–11</sup> because of their importance in many fields of application, e.g., electronic devices, storage media, inkjet printing, paint technology, micro- and nanoscale array fabrications, and biosensors. Proper knowledge of the intermolecular and external forces is needed to continue improving the production of desired nano- and microstructured materials through self- and directed assembly.<sup>12</sup> Controlled evaporation of droplets with proper solutes provides a simple route for self-assembled formations. A well-known example of pattern formation of micro- and nanoparticles caused by droplet evaporation is the so-called “coffee ring” or “rings”, where a spilled drop of coffee dries on a solid surface and leaves a dense, ring-like deposit of particles along the perimeter of the original drop.<sup>1</sup> Other studies show that particles can self-assemble into either filaments parallel<sup>13</sup> or perpendicular<sup>14</sup> to the boundary line of the evaporating droplet. The range of pattern formations can be greatly expanded through active (e.g., electric and/or magnetic fields) and passive (e.g., templated surfaces) directed assembly, as well as using hydrodynamic, such as fingering, instabilities, at the air–liquid–solid (ALS) interface.<sup>15–17</sup> Recently, the substrate geometry (e.g., confinement between two surfaces) has been used as a passive directed-assembly mechanism.<sup>18–20</sup> One

of the advantages of solution confinement is that the solution is held by capillary forces, as opposed to spreading on the wetting surface.

CNTs have remarkable electronic and mechanical properties. Since the pioneering reports on the preparation of carbon filaments with very small diameter ( $<10$  nm) in 1976, the synthesis and assembly of CNTs have steadily progressed.<sup>11,21–23</sup> Aligned CNT thin films have many potential applications in flexible transparent electrodes and displays and various sensors. The development of cheap flexible displays has been a major challenge for researchers and the whole display industry. Most traditional materials and processes commonly used for today’s flat panel displays cannot be transferred to flexible substrates; for example, indium tin oxide (ITO), amorphous or polycrystalline silicon, used traditionally for transparent and conductive coatings, or thin film transistors are brittle and cannot be bent. The patterned CNT thin layer can be used as an effective means for liquid crystal aligning and used as transparent electrodes for flexible displays, which can be applied in cell phones, biosensors, and electronic books and magazines. The current strategies for the assembly of CNTs mainly include chemical synthesis, such as chemical vapor deposition (CVD),<sup>24</sup> and physical methods, such

Received: February 4, 2011

Revised: April 28, 2011

Published: May 10, 2011

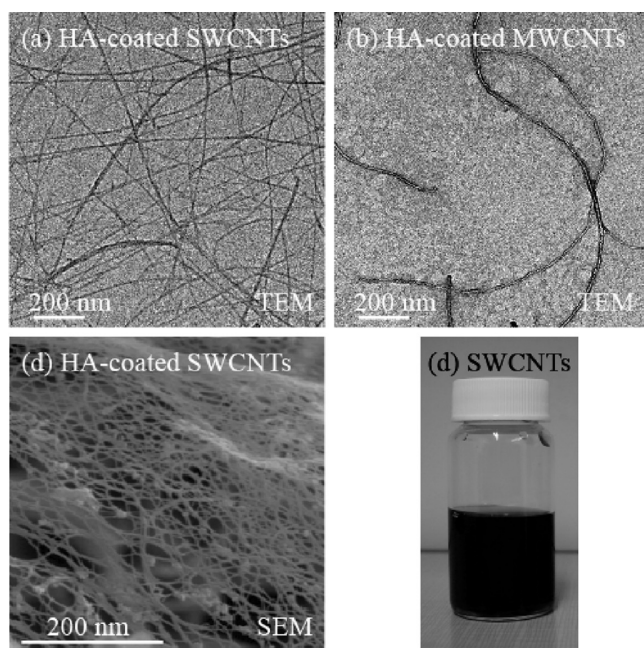


**Figure 1.** TEM images of HA-coated (a) SWCNTs (53 mg/L) and (b) MWCNTs (36 mg/L). (c) SEM image of freeze-dried HA-coated SWCNTs. (d) Photo of HA-coated SWNT dispersion at a concentration of 53 mg/L, which is very stable, and no significant phase separation or aggregation was observed, even after 1 month.

as forced patterning by flow<sup>25</sup> or shear,<sup>26</sup> trapping in template surfaces,<sup>27</sup> or applying electric or magnetic fields.<sup>6,11</sup> Some of these methods involve complicated, costly, and multi-step procedures. Here, we report a simple method to achieve large areas (>mm<sup>2</sup>) of textured CNT patterns, of both single-walled carbon nanotubes (SWCNTs) and multiwalled carbon nanotubes (MWCNTs), through droplet evaporation, making use of special geometry of the substrate surface.

## MATERIALS AND METHODS

Highly purified 2 nm diameter SWCNTs synthesized by the HiPco process were obtained from Tubes@Rice and were used as received. MWCNTs, produced by CVD, of purity >90% and less than 0.1% metal (Fe) content, purchased from MER Corp., were also used as received. The MWCNTs are 25 ± 10 nm in diameter. Humic acid (HA) was purchased from MP Biomedicals, Inc., with purity >99%.

It was recently shown that natural organic matter, such as HA, is a very good dispersant of CNTs, requiring a much smaller amount of HA than conventional surfactants, such as sodium dodecyl sulfate (SDS), to disperse the same amount of CNTs.<sup>28</sup> HA is composed of 49.5 wt % carbon, 43.3 wt % oxygen, and 5.1 wt % hydrogen. The exact molecular structure of HA is still unknown.<sup>29</sup> HA is usually considered as a natural surfactant, containing aromatic rings and abundant hydrophilic functional groups, such as carboxylic acid and phenolic groups.<sup>29</sup>

The HA-coated CNT suspension was prepared following our recent report.<sup>30</sup> Basically, a stock solution was prepared by dissolving an appropriate amount of HA solid in deionized (DI) water and filtering the solution through a 0.45 μm pore-size membrane. The HA-coated CNT dispersion was prepared by adding a constant amount (e.g., 5–10 mg) of SWCNTs or MWCNTs into 30 mL of a HA solution (10–25 mg/L). The HA–CNT mixtures were then sonicated using a low-power bath sonicator (50 W) for 60 min, followed by agitation in an end-over-end shaker at 60 rpm for 24 h. The mixtures were then centrifuged at 10 000

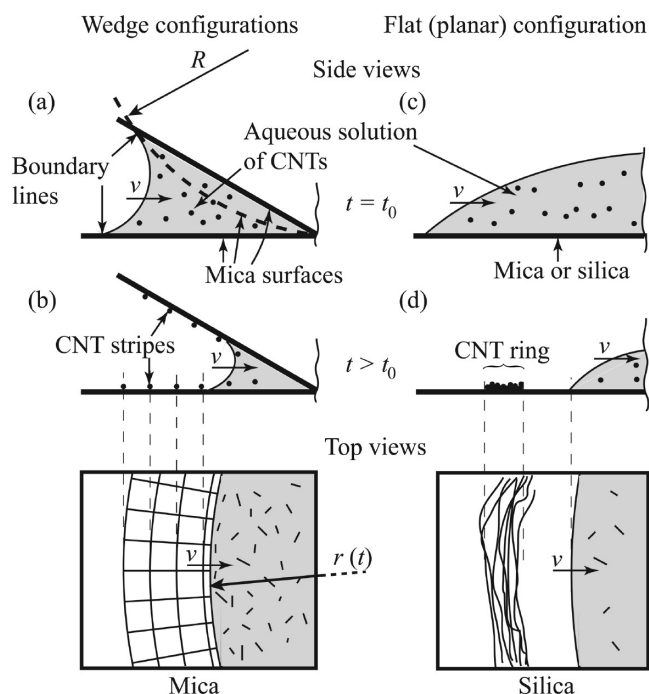


**Figure 2.** Effect of the evaporation of aqueous dispersion of HA-coated CNTs in different types of substrate surface geometries. In (a), the solid line shows the wedge configuration, while the dotted line indicates the curved-wedge (or sphere-on-flat) configuration, with a sphere of radius of curvature  $R$ . An aqueous droplet of CNT is placed on the surface in these geometries at initial time  $t_0$ . The boundary line of the evaporating droplet or the ALS interface moves with velocity  $v(t)$  as the water evaporates until all of the water has evaporated at time  $t_f$ . (a and b) CNT sediment forms an ordered pattern of stripes on the surface if the surface geometry is either a curved wedge or wedge. (c and d) CNT sediment forms “coffee ring” structures (on silica) or random clusters (on mica) if the surface geometry is a single flat (planar) surface.

relative centrifugal force (RCF) to remove undispersed CNT aggregates, and the supernatant, containing stably dispersed CNTs, was carefully decanted for further analysis. The HA-coated CNT suspension was very stable. No significant phase separation or aggregation of CNTs was observed, even after 1 month. The stable CNT dispersion solutions were further filtered through a 1.6 μm filter right before the experiments. The concentration of the HA-wrapped CNTs was determined by a freeze-drying and weighing method reported recently.<sup>30</sup> Ultraviolet–visible (UV–vis) absorption spectroscopy was also used to determine the dispersion of CNTs in aqueous solution in the presence of HA. The concentration of HA-coated CNTs was determined by measuring the absorbance of the solution at 600 nm and using an extinction coefficient of  $2.23 \times 10^4$  cm<sup>2</sup>/g for SWNTs and  $2.88 \times 10^4$  cm<sup>2</sup>/g for MWNTs, which were determined experimentally for the same CNT samples as reported recently.<sup>30</sup> Transmission electron microscopy (TEM) was used to visualize the structure of HA-coated SWCNTs and MWCNTs used in our study. As shown in Figure 1, SWNTs were exfoliated into thin bundles, while MWNTs were completely isolated in HA solution.

The evaporation of a droplet of the aqueous CNT dispersion was performed in three different substrate geometries: curved wedge, wedge, and single flat only. The first two geometries give a concave meniscus of the aqueous droplet with the surface, while the latter geometry gives a convex meniscus. The curved-wedge (sphere-on-flat) geometry (see Figure 2a) was achieved in a surface force apparatus (SFA).<sup>31</sup> Atomically smooth 1–4 μm thick sheets of back-silvered muscovite mica (S&J Trading, Glen Oaks, NY) were glued to cylindrical silica disks (disk



radius  $r_{\max} = 5$  mm and radius of curvature  $R = 20$  mm) with epoxy (Shell Epon 1004) glue, where the back-silvered 500–550 Å thick silver layer was used as the reflecting layer to produce fringes of equal chromatic order (FECO) to measure surface separations and deformations. The two disk-supported mica sheets were mounted into the SFA chamber and brought into contact in the geometry of crossed cylinders, and a finite load was applied to achieve a flat contact of diameter  $\sim 150$   $\mu\text{m}$ . This crossed-cylinder geometry corresponds to a sphere of radius  $R$  on a flat surface<sup>32</sup> when the minimum distance between the two surfaces is much less than the radius  $R$ . A drop (50–100  $\mu\text{L}$ ) of HA-coated SWCNT (or MWCNT) dispersion was injected into the gap between the two mica surfaces, which produced a capillary bridge. The aqueous dispersion was evaporated by slowly purging dry  $\text{N}_2$  through the chamber. The evaporation generally took a few hours to complete.

In a separate experiment, two freshly cleaved mica sheets was positioning in a wedge of about  $10^\circ$  and  $30^\circ$  (see Figure 2a). These wedges were filled with several drops (100–500  $\mu\text{L}$ ) of HA-coated CNT dispersion and left to dry in air ( $\sim 70\%$  humidity). The third type of experiment was simply depositing a drop of CNT dispersion on a freshly cleaved mica sheet or a precleaned silica wafer, which was placed in a horizontal position (Figure 2c) and dried in a  $\text{N}_2$  atmosphere. After the drying procedure, all of the surfaces were characterized by optical microscopy (a Nikon OPTIPHOT 200 microscope) and atomic force microscopy (AFM). All experiments were performed at room temperature ( $20^\circ\text{C}$ ).

## RESULTS AND DISCUSSION

CNTs sediment out of an aqueous solution as water evaporates from the dispersion. For certain geometries of the substrate surface, the layers of dried CNTs on the surfaces form ordered structures (Figure 2). Ordered lattice-like patterns with filaments of CNTs in both perpendicular and parallel to the boundary line of the evaporating droplet are observed here after evaporation of CNT dispersion in wedge and curved-wedge configurations (Figure 2a). Panels a–c of Figure 3 show optical microscopy and AFM images of selected parts of rings of radius  $r$  (cf. Figure 2) of the patterned surfaces of SWCNTs and MWCNTs on mica in the curved-wedge configurations. The patterns clearly display clustering of CNTs into both concentric rings and radial filaments, which form up to  $\text{mm}^2$  large lattice-like structures. The width of the filaments is 2–10  $\mu\text{m}$  in both directions, and the center–center distance between two filaments is also 2–10  $\mu\text{m}$  in both directions. The farther the pattern is away from the contact center, the larger the (characteristic) dimensions of the lattice.

Drying droplets of CNT dispersion in a  $30^\circ$  wedge configuration of two freshly cleaved mica sheets also produce a 2D lattice pattern of CNT (Figure 3d). However, the majority of the filaments are perpendicular to the boundary line of the evaporating droplet. A  $10^\circ$  wedge configuration was also tested. The phenomena observed and patterned surfaces formed were similar, although it gave a slightly ( $\sim 20\%$ ) higher fraction of filaments perpendicular to the boundary line than in the  $30^\circ$  case (not shown). As for the curved-wedge configuration, the dimensions of the resulting lattice are smaller as the boundary line of the evaporating droplet approaches the intersection of the two mica sheets.

The importance of the special constrained geometry was tested by a comparison to the flat substrate surface geometry case (Figure 2d). In this case, no ordered structure was formed on either mica sheets or silica wafers. On non-wetting silica wafers, “coffee rings” at the initial boundary of the droplet were formed together with sparsely disordered aggregates located near

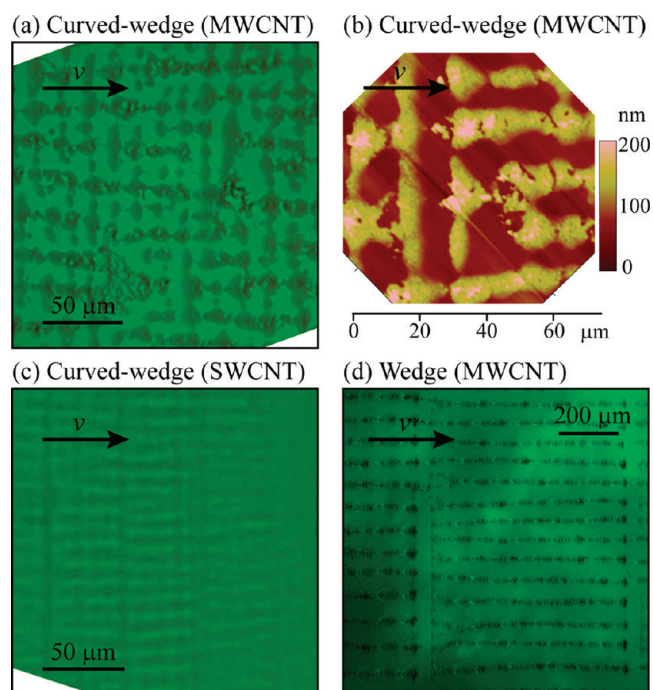


**Figure 3.** Microscope and AFM images of evaporation-induced self-ordered CNT films on mica surfaces in the curved-wedge (sphere-on-flat) and wedge configurations. Droplets in the curved-wedge configuration give patterns of (a) MWCNTs and (c) SWCNTs. (b) AFM image of a. (d) Evaporation of droplets of MWCNT dispersion in a  $30^\circ$  wedge produce lattice formation of filaments oriented both parallel and perpendicular to the boundary line of the evaporating droplet, with a majority of perpendicular clusters.

the center of the droplet. On flat mica, the dispersion readily wets and large aggregates of CNT were found distributed randomly but close to the center of the initial drop.

The main difference between wedge and single flat configurations is the meniscus formed at the ALS interface (the contact angle is the same for mica in all configurations). The evaporation of the convex droplet in the single flat configuration leads to a flow of dispersed nanoparticles to the boundary line of the droplet only,<sup>1</sup> while a concave droplet in the wedge configurations has less liquid area exposed to air, which reduces the flow of CNTs to the ALS interface.

The observed patterns of CNT dispersion after the evaporation of a concave droplet follow two competing or cooperative sedimentation mechanisms occurring at the boundary line of the evaporating droplet, as illustrated and exemplified in Figure 4. First there are the capillary forces between the CNTs, which give clusters of CNTs *parallel* to the boundary line of the droplet, and second there are the fingering instability and subsequent pinning of CNTs, leading to clusters of CNTs aligned *perpendicular* to this boundary line.

The first mechanism assumes a radial transport of CNTs from the bulk (thick film) region to the shallow (thin film) regions as the water evaporates from the capillary bridge between the bifurcating mica surfaces (Figure 4a).<sup>33</sup> However, these particles do not settle until they reach the droplet boundary line, where they cluster together. As the water evaporates further, the water at the boundary line is too shallow for more particles to access the cluster, which leads to a formation of new clusters closer to the center. Figure 5 shows the schematic of the CNT clustering

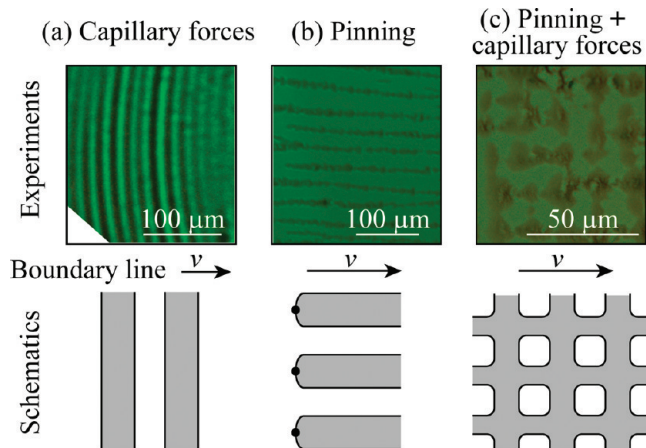


**Figure 4.** Two main processes in forming structural films of nanoparticles on the surfaces. (a) Particles trapped on the surface because of surface tension and capillary attractive forces, which form sedimented filaments parallel to the boundary line of the evaporating droplet, and (b) fingering instability at the boundary line and subsequent pinning of CNTs on the surface induce a cascade of sedimented particles along the wake after the pinned CNTs as the droplet evaporates. (c) When these two processes are combined, we obtain a 2D lattice of sedimented particles. Images in the top row are optical microscope pictures from curved-wedge geometry experiments; the bottom row shows schematics of the above images. The boundary lines move from left to right in all three cases, as indicated by the arrows.

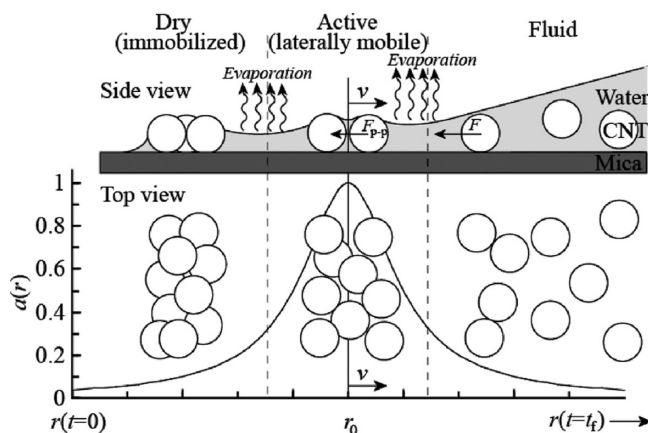


**Figure 5.** Schematic side view of CNTs clustering near the boundary line of an evaporating droplet because of the capillary forces. The boundary line of the evaporating droplet is defined at  $r_0$  and moves to the right with velocity  $v$  as the water evaporates. The CNTs are pulled toward  $r_0$  by capillary force  $F_{p-p}$ , which can be modeled to be proportional to the parameter  $a(r)$  in Stokes drag (eqs 1–3). In the fluid region, the CNTs are assumed to be randomly distributed. In the dry region, a region already visited by the water front, the CNTs form clusters and are immobilized because of the low water level.

process. The CNTs in the water solution (fluid state) are assumed to be randomly distributed. The motion of CNTs in water is strongly damped by the water viscosity. Therefore, the velocity of the particles/cluster  $u$  is to a first order of approximation proportional to the force  $F_{p-p}$  acting on them (no acceleration) or simply given by the Stokes drag

$$u = aF_{p-p} \quad (1)$$

where  $a$  is a proportionality factor. The forces acting on each CNT varies with several parameters, such as the wetting properties of the CNT, the shape of the water surface, and dispersion composition. The dominating interaction force is the attractive capillary forces between the CNT  $F_{p-p}$ , which is inversely proportional to the center–center distance  $d$  between them

$$F_{p-p} \sim -\frac{2\pi R_1 R_2 \gamma_{H_2O}}{d} \quad (2)$$

where  $R_1$  and  $R_2$  are the radius of the particles/clusters and  $\gamma_{H_2O}$  is the surface tension of water. The attractive interparticle forces are strongest in an active region (see Figure 5). We can assume that the proportionality factor  $a$  is a function of the radial  $r$  coordinate with a central peak  $r_0$  and decays rapidly to 0 away from the active region (Figure 5). Several functions can be used to exemplify the active region. Figure 5 shows

$$a(r) \propto \frac{1}{1 + (r - r_0)^2} \quad (3)$$

Fujita et al.<sup>34</sup> have shown computer simulations on two-dimensional self-organization of nanoparticles in liquid films, which used a similar model described above by eqs 1–3 and Figure 5. Following the above model, computer simulations on the evaporation of CNT dispersions in this study should be able to give a qualitative understanding of pattern formation parallel to the boundary line of the evaporating droplet, which, however, is beyond the scope of this paper.

The second mechanism is more subtle and involves both a fingering instability of the boundary line of the evaporating droplet and the interaction forces between the CNTs and the mica substrate. As the flow of CNTs reaches the droplet boundary line, the local concentration of CNTs increases. The attractive van der Waals forces between the CNTs eventually overcome the HA-induced repulsive electrostatic forces between the CNTs and, thus, drive the CNTs to cluster together. As the water further evaporates, fingering instability, which is caused by many interplaying factors, including capillary (surface tension), hydrodynamic, van der Waals, and electrostatic forces, thermal and concentration gradients of the solvent, CNTs and dissolved HA molecules, and surface roughness,<sup>15,16,35–37</sup> eventually divides the CNT clusters in regions of lowest density. Also, the HA coating (HA contains both hydrophilic groups that bind to mica and hydrophobic groups that bind to the CNT) mediates an adhesive force between the CNTs and mica sheet, which can pin down a CNT and generate a nucleation point for further settlement of CNTs in the wake of this pinning point, as seen in Figure 4b.

When these two mechanisms of sedimentation are combined at the surface in the wedge configurations, the sedimentation of CNTs forms lattice-like formations on the surface, as shown in Figure 4c. The exact formation depends upon the interparticle forces between the dispersed CNTs in aqueous solution and the geometry of the substrate surface. The interparticle forces can be modulated by changing the pH, salt concentration, salt type and valency, and substrate property.<sup>32,38,39</sup> When these possibilities of modulations are explored, together with the proper geometric configuration of the substrate surface, it is possible to gain better control of the pattern formation.

## CONCLUSION

Our data demonstrate the possibility of evaporation-induced lattice-like pattern formation of CNTs from an aqueous dispersion

in special geometries of the substrate surface(s). Optimizing the evaporation procedure, dispersion composition, and substrate surface geometry provides better control of the pattern formation of CNTs, as well as the possibility to target specific patterns for different applications. For example, one could ideally obtain large areas of straight-aligned lattice patterns using a wedge-shaped tape-peeling geometry with controlled peeling speed and angle. Also, further experiments have to be carried out to investigate the orientation and connectivity of the CNTs within the patterned clusters, which are important for possible applications of specialized formations of CNTs.

## AUTHOR INFORMATION

### Corresponding Author

\*E-mail: hongbo.zeng@ualberta.ca (H.Z.); jacob@engineering.ucsb.edu (J.I.).

### Present Addresses

<sup>†</sup> Division of Chemical and Life Sciences and Engineering, King Abdullah University of Science and Technology (KAUST), Thuwal 23955-6900, Kingdom of Saudi Arabia.

### Author Contributions

<sup>†</sup> These authors contributed equally to this work.

## ACKNOWLEDGMENT

This work was supported by the Division of Materials Sciences, U.S. Department of Energy, under Award DE-FG02-87ER-45331. Hongbo Zeng thanks the support of a Discovery Grant from the Natural Sciences and Engineering Research Council of Canada (NSERC).

## REFERENCES

- Deegan, R. D.; Bakajin, O.; Dupont, T. F.; Huber, G.; Nagel, S. R.; Witten, T. A. *Nature* **1997**, 389, 827.
- Ghosh, M.; Fan, F. Q.; Stebe, K. J. *Langmuir* **2007**, 23, 2180.
- Hong, S. W.; Xia, J. F.; Lin, Z. Q. *Adv. Mater.* **2007**, 19, 1413.
- Kim, J. W.; Larsen, R. J.; Weitz, D. A. *J. Am. Chem. Soc.* **2006**, 128, 14374.
- Lin, Z. Q.; Granick, S. *J. Am. Chem. Soc.* **2005**, 127, 2816.
- Long, D. P.; Lazorcik, J. L.; Shashidhar, R. *Adv. Mater.* **2004**, 16, 814.
- Mokari, T. L.; Zhang, M. J.; Yang, P. D. *J. Am. Chem. Soc.* **2007**, 129, 9864.
- Nikolaides, M. G.; Bausch, A. R.; Hsu, M. F.; Dinsmore, A. D.; Brenner, M. P.; Weitz, D. A.; Gay, C. *Nature* **2002**, 420, 299.
- Schuth, F.; Ciesla, U.; Schacht, S.; Thieme, M.; Huo, Q.; Stucky, G. *Mater. Res. Bull.* **1999**, 34, 483.
- Sethi, S.; Ge, L.; Ci, L.; Ajayan, P. M.; Dhinojwala, A. *Nano Lett.* **2008**, 8, 822.
- Yan, Y. H.; Chan-Park, M. B.; Zhang, Q. *Small* **2007**, 3, 24.
- Min, Y. J.; Akbulut, M.; Kristiansen, K.; Golan, Y.; Israelachvili, J. *Nat. Mater.* **2008**, 7, 527.
- Xu, J.; Xia, J. F.; Lin, Z. Q. *Angew. Chem., Int. Ed.* **2007**, 46, 1860.
- Huang, J. X.; Kim, F.; Tao, A. R.; Connor, S.; Yang, P. D. *Nat. Mater.* **2005**, 4, 896.
- Leizerson, I.; Lipson, S. G.; Lyushnin, A. V. *Langmuir* **2004**, 20, 291.
- Lyushnin, A. V.; Golovin, A. A.; Pismen, L. M. *Phys. Rev. E: Stat. Phys., Plasmas, Fluids, Relat. Interdiscip. Top.* **2002**, 65, No. 021602.
- Yabu, H.; Shimomura, M. *Adv. Funct. Mater.* **2005**, 15, 575.
- Byun, M.; Bowden, N. B.; Lin, Z. Q. *Nano Lett.* **2010**, 10, 3111.
- Hong, S. W.; Byun, M.; Lin, Z. Q. *Angew. Chem., Int. Ed.* **2009**, 48, 512.
- Xu, J.; Xia, J.; Hong, S. W.; Lin, Z.; Qiu, F.; Yang, Y. *Phys. Rev. Lett.* **2006**, 96, No. 066104.
- Oberlin, A.; Endo, M.; Koyama, T. *Carbon* **1976**, 14, 133.
- Oberlin, A.; Endo, M.; Koyama, T. *J. Cryst. Growth* **1976**, 32, 335.
- Iijima, S. *Nature* **1991**, 354, 56.
- Fan, S. S.; Chapline, M. G.; Franklin, N. R.; Tomblor, T. W.; Cassell, A. M.; Dai, H. J. *Science* **1999**, 283, 512.
- Huang, Y.; Duan, X. F.; Wei, Q. Q.; Lieber, C. M. *Science* **2001**, 291, 630.
- Vigolo, B.; Penicaud, A.; Coulon, C.; Sauder, C.; Pailler, R.; Journet, C.; Bernier, P.; Poulin, P. *Science* **2000**, 290, 1331.
- Hong, S. W.; Jeong, W.; Ko, H.; Kessler, M. R.; Tsukruk, V. V.; Lin, Z. Q. *Adv. Funct. Mater.* **2008**, 18, 2114.
- Hyung, H.; Fortner, J. D.; Hughes, J. B.; Kim, J. H. *Environ. Sci. Technol.* **2007**, 41, 179.
- VanLoon, G. W.; Duffy, S. J. *Environmental Chemistry: A Global Perspective*, 2nd ed.; Oxford University Press: New York, 2005.
- Wang, P.; Shi, Q. H.; Liang, H. J.; Steuerman, D. W.; Stucky, G. D.; Keller, A. A. *Small* **2008**, 4, 2166.
- Israelachvili, J.; Min, Y.; Akbulut, M.; Alig, A.; Carver, G.; Greene, W.; Kristiansen, K.; Meyer, E.; Pesika, N.; Rosenberg, K.; Zeng, H. *Rep. Prog. Phys.* **2010**, 73, No. 036601.
- Israelachvili, J. *Intermolecular and Surface Forces*, 2nd ed.; Academic Press: New York, 1991.
- Denkov, N. D.; Velev, O. D.; Kralchevsky, P. A.; Ivanov, I. B.; Yoshimura, H.; Nagayama, K. *Nature* **1993**, 361, 26.
- Fujita, M.; Nishikawa, H.; Okubo, T.; Yamaguchi, Y. *Jpn. J. Appl. Phys., Part 1* **2004**, 43, 4434.
- Troian, S. M.; Wu, X. L.; Safran, S. A. *Phys. Rev. Lett.* **1989**, 62, 1496.
- Cazabat, A. M.; Heslot, F.; Troian, S. M.; Carles, P. *Nature* **1990**, 346, 824.
- Fanton, X.; Cazabat, A. M. *Langmuir* **1998**, 14, 2554.
- Lange, F. F. *J. Am. Ceram. Soc.* **1989**, 72, 3.
- Niyogi, S.; Boukhalfa, S.; Chikkannanavar, S. B.; McDonald, T. J.; Heben, M. J.; Doorn, S. K. *J. Am. Chem. Soc.* **2007**, 129, 1898.